Microtubule Sliding in Swimming Sperm Flagella: Direct and Indirect Measurements on Sea Urchin and Tunicate Spermatozoa

Charles J. Brokaw

Division of Biology, California Institute of Technology, Pasadena, California 91125

Abstract. Direct measurements of microtubule sliding in the flagella of actively swimming, demembranated, spermatozoa have been made using submicron diameter gold beads as markers on the exposed outer doublet microtubules. With spermatozoa of the tunicate, *Ciona*, these measurements confirm values of sliding calculated indirectly by measuring angles relative to the axis of the sperm head. Both methods of measurement show a nonuniform amplitude of oscillatory sliding along the length of the flagellum, providing direct evidence that "oscillatory synchronous sliding" can be occurring in the flagellum, in addition to the metachronous sliding that is necessary to propagate a bending wave. Propagation of constant amplitude bends is not accomplished by propagation of a wave of oscillatory sliding of constant amplitude, and therefore appears to require a mechanism for monitoring and controlling the bend angle as bends propagate.

With sea urchin spermatozoa, the direct measurements of sliding do not agree with the values calculated by measuring angles relative to the head axis. The oscillation in angular orientation of the sea urchin sperm head as it swims appears to be accommodated by flexure at the head–flagellum junction and does not correspond to oscillation in orientation of the basal end of the flagellum. Consequently, indirect calculations of sliding based on angles measured relative to the longitudinal axis of the sperm head can be seriously inaccurate in this species.

Sea urchin and tunicate spermatozoa propagate nearly planar bending waves along their flagella. The propagation of the bending waves is associated with propagation of regions of sliding between axonemal microtubules, with the direction of sliding reversing as the direction of curvature of the flagellum reverses (Brokaw, 1971). This distribution of microtubule sliding in flagella has not been deduced by direct observations of sliding, but by observations of bending of the flagellum. As illustrated in Fig. 1, the sliding between outer doublet microtubules can be calculated from the bent configuration of the flagellum, assuming that there is no twisting of the axoneme or longitudinal compliance of the microtubules. With these assumptions, the amount of sliding between two outer doublet microtubules at a particular locus on the flagellum is proportional to the difference in angular orientation between that locus and the basal end of the flagellum, where there is assumed to be no sliding (Satir, 1968; Warner and Satir, 1974; Gibbons, 1981). The constant of proportionality is the "doublet separation": the distance, in the plane of bending, between the two sliding outer doublet microtubules. Since this will vary depending upon the choice of microtubules, it is convenient to describe the pattern of sliding in terms of "shear angle," measured in angular units (rads), without introducing a proportionality constant. Sets of shear angle curves, showing the shear angle as a function of position along the flagellum, for various times in the beat cycle, thus provide a useful description of the sliding occurring in a flagellum.

Fig. 2 *A* shows a set of shear angle curves for a hypothetical flagellar bending pattern composed of circular arcs. It shows the pattern of propagated sliding that has been referred to as "metachronous" sliding (Brokaw and Gibbons, 1975; Goldstein, 1976), with a uniform amplitude of oscillatory sliding at each position in the distal portion of the flagellum. Sliding associated with the growth (i.e., increase in angle) of a bend at the base of a flagellum has been referred to as "synchronous" sliding, because it corresponds to a constant velocity of sliding throughout the portion of the flagellum distal to the growing bend. The basal region of these sperm flagella normally contains two developing bends. In many cases, these two developing bends have approximately equal rates of increase of bend angle in opposite directions, so that the summed synchronous sliding required by these two developing bends is relatively small, and does not greatly alter the pattern of primarily metachronous sliding in bends propagating along the distal regions of the flagellum (Goldstein, 1976).

With light microscopy, determining the orientation of the basal end of a flagellum is difficult. In dark-field photomicrographs, the sperm head image interferes with observation of

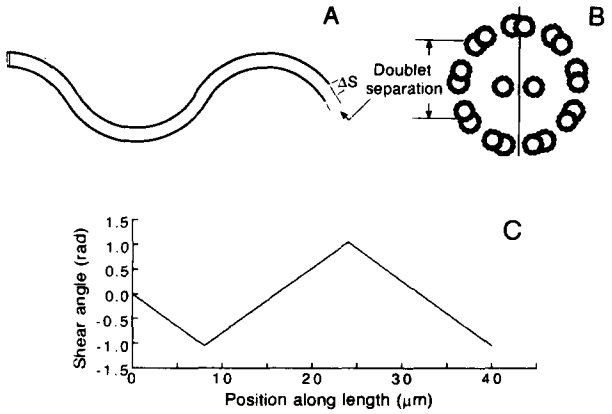

Figure 1. Bending and sliding in a hypothetical flagellar bending pattern composed of circular arcs. In *A*, the two parallel lines represent two outer doublet microtubules, tied firmly together at their basal (*left*) ends, which slide relative to one another as the flagellum bends. This diagram is not to scale; the distance between the doublets has been greatly exaggerated relative to the lengths and radii of curvature of the bends. *B* shows the arrangement of microtubules seen in a cross-section of an axoneme. The "doublet separation" between any two outer doublets (in this case doublets 7 and 9) is the distance between the doublets, projected onto the bending plane shown by the vertical line. *C* shows shear angle values as a function of length along the flagellum for the bending pattern in *A*. The "shear angle" at any point is the angle of a tangent to the flagellum at that point, measured relative to the direction of the basal end of the flagellum, where there is no sliding between the microtubules. Absolute amounts of sliding, indicated in *A* by ΔS, can be obtained by multiplying the shear angle by the doublet separation. For this simple hypothetical waveform, each bend on the flagellum is represented by an inclined line in the shear angle plot.

the basal end of the flagellum. Even in cases where the sperm head detaches, leaving behind a fully motile flagellum, bending typically occurs so close to the basal end that there is no straight region at the basal end of sufficient length for accurate measurement of its orientation (see Sale, 1986). For these reasons, many studies of sperm flagellar motility have used the longitudinal axis of the sperm head as a reference orientation for determining shear angles, assuming that this axis remains at a constant angle to the base of the flagellum during the beat cycle. The patterns of sliding calculated in this manner for freely swimming spermatozoa often resemble the pattern illustrated in Fig. 2 *C*, indicating that the amplitude of sliding is not constant along the length of the flagellum (Hiramoto and Baba, 1978; Brokaw, 1979; Gibbons, 1981, 1982; Omoto and Brokaw, 1982). Such patterns can be interpreted to indicate the presence of a minor but significant component of synchronous sliding superimposed on metachronous sliding with constant amplitude. This form of synchronous sliding, illustrated in Fig. 2 *B*, has been termed "oscillatory synchronous sliding" to distinguish it from a nonoscillatory component associated with asymmetric bending waves (Gibbons, 1981). It has been suspected that this apparent oscillatory synchronous sliding might be an artifact resulting from changes in orientation of the base of the flagellum relative to the head axis (Brokaw, 1979; Gibbons, 1981), but until now there has been no independent method for measuring sliding that would allow the evaluation of this possibility.

In this paper, a new method (Brokaw, 1989*a*) is used for direct measurement of microtubule sliding in beating flagella by measuring the movements of gold beads attached to the exposed outer doublet microtubules of demembranated flagella. This method is applied here to demembranated spermatozoa of a sea urchin, *Lytechinus*, and a tunicate, *Ciona*, reactivated with MgATP to beat at relatively high beat frequencies where there is significant oscillation in orientation of the sperm head during swimming. For *Lytechinus* spermatozoa, this new method indicates a flexible attachment of the sperm head to the flagellum, so that angles measured relative to the sperm head do not give an accurate picture of

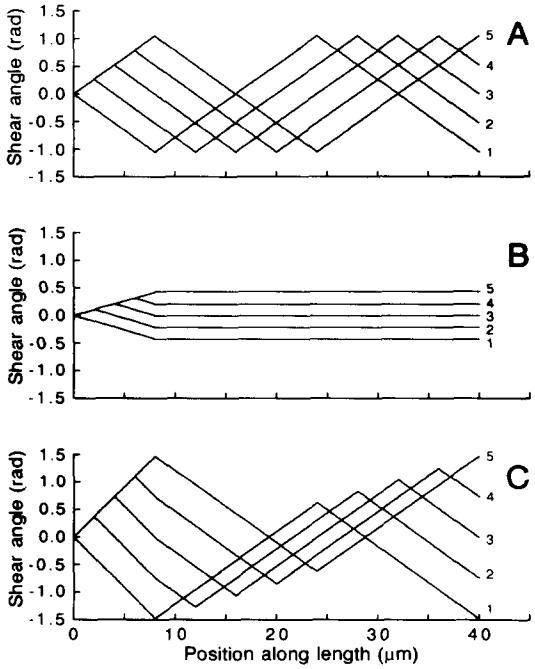

Figure 2. Shear angle curves for hypothetical flagellar bending patterns composed of circular arcs, as in Fig. 1, *A* and *C*. Each set contains five shear curves covering one-half of a beat cycle, at one-eighth cycle intervals. The vertical distance between successive curves therefore represents the sliding occurring during a one-eighth-cycle time interval. *A* represents the pattern described as metachronous sliding, with each bend growing to half its final angle of 2.1 rad during the first half of a beat cycle and completing its growth at the same rate during the next half-cycle. After completing its growth, each bend propagates in association with a shear angle oscillation having a uniform amplitude of 1.05 rad at each point along the length. This corresponds to a "square wave" sliding oscillation at a constant rate of 4.2 rad/cycle for 0.5 cycle and at −4.2 rad/cycle for 0.5 cycle. *B* represents a pattern of synchronous sliding, with the growth of the bend at the basal end associated with a uniform increase in shear angle at all points distal to the growing bend. The amplitude of oscillatory synchronous sliding is 0.42 rad. *C* is the sum of the metachronous sliding in *A* and the synchronous sliding in *B*. The bend angle, measured by the vertical distance between the ends of the propagating bends, remains constant at 2.1 rad as the bends propagate. However, the shear angle amplitude varies along the length. For this example, the phase relationship between the two sliding components has been chosen so that the synchronous component uniformly increases the rate of growth of bend angle during the first half-cycle of bend growth. This results in maximum shear angle amplitudes of 1.47 rad at 8 and 40 μm from the basal end and a minimum shear angle amplitude of 0.63 rad at 24 μm from the basal end.

sliding in the flagellum. For *Ciona* spermatozoa, the measurements validate the sliding patterns obtained by measuring angles relative to the sperm head axis, and verify the presence of oscillatory synchronous sliding associated with bend propagation by these sperm flagella.

Materials and Methods

Flagellar Preparations

Sea urchin spermatozoa were collected from *Lytechinus pictus*, and stored on ice without dilution until used (up to 4 h). For each microscope sample, 2 μl of concentrated spermatozoa were mixed with 100 μl of demembranation solution containing 250 mM KCl, 10 mM Tris-HCl buffer (pH 8.2), 1 mM DTT, 2 mM $MgSO_4$, 1 mM EGTA, and 0.04% Triton X-100. After 30 s, 300 μl of activation solution containing 50 mM KCl, 10 mM Tris-HCl (pH 8.2), 1 mM DTT, 0.5 mM $MgSO_4$, 1 mM ATP, and 10 μM cAMP was added. After 2 min, 5 μl of 0.2 M $CaCl_2$ was added to this mixture to extract calmodulin and give more symmetric bending waves on reactivation (Brokaw and Nagayama, 1985). After an additional 20 s, 100 μl of this mixture was added to 1 ml of bead adhesion solution. This was a mixture of nine parts of solution containing 250 mM potassium acetate, 20 mM Tris-HCl (pH 8.2), 1 mM DTT, 1 mM EGTA, and 0.44 mM $MgSO_4$, with one part of solution containing 40 nm gold beads, either the suspension as supplied by Janssen Life Science Products (Piscataway, NJ) or a more concentrated suspension obtained by gentle centrifugation. The bead suspension was added to this solution immediately before the addition of the demembranated sperm suspension. After 1–2 min, a 100-μl portion of this solution was mixed with 1 ml of reactivation solution containing 250 mM potassium acetate, 20 mM Tris-HCl (pH 8.2), 1 mM DTT, 2 mM EDTA, 2.27 mM $MgSO_4$, 0.12 mM ATP, 2 mM lithium acetate, 0.5% polyethylene glycol, and 0.12% methyl cellulose (4,000 cp; Fisher M-281). This solution is designed to have a MgATP concentration of 80 μM. Lithium ion was included in these solutions to increase the bend angle (Brokaw, 1987, 1989*b*). Small amounts of $CaCl_2$ were also added to obtain free Ca^{2+} concentrations in the range of 10^{-8} to 10^{-7} M, to modify the asymmetry of the bending waves.

Spermatozoa from the tunicate, *Ciona intestinalis*, were prepared and decorated with beads in a similar manner, following demembranation and reactivation procedures described previously (Brokaw, 1987), except that the pH was reduced to 7.6. The reactivation solution was similar to that used for *Lytechinus* spermatozoa, with 0.3 mM Mg^{2+}, 0.4 mM MgATP, 1.0–1.2 mM lithium acetate, and 0.05% methyl cellulose. Lithium ion was included in these solutions to obtain a mixture of propagating and damped bending wave patterns (Brokaw, 1987), but only the propagating patterns are considered here.

Spermatozoa were observed in thin, hanging drop preparations (Brokaw and Benedict, 1968). A well slide was made by cutting a 14.5-mm diameter hole in a piece of 1.35-mm aluminum sheet. The bottom of the hole was covered with a no. 1 round cover glass, affixed with epoxy cement. The well was filled with mineral oil. A thin drop of spermatozoa in reactivation solution was spread over the lower surface of a cover glass, and placed on top of the well without trapping any air bubbles. Spermatozoa were observed and photographed at the oil-water interface using a Zeiss 100× oil immersion objective, with iris diaphragm, and a Zeiss ultra dark field condenser. Stroboscopic illumination at 120 flashes per second (*Lytechinus*) or 280 flashes per second (*Ciona*) was provided by an LX150F lamp (ILC Technology, Sunnyvale, CA), operated in pulsed mode by a model 136 power supply (Chadwick-Helmuth, El Monte, CA) (Brokaw, 1986). Photographs were taken on Kodak Tri-X or TMax 3200 35-mm film in an oscilloscope camera operated at a film speed of 0.5 or 1 m/s, with 0.5- or 0.2-s exposures recording ~50 sperm images (Brokaw, 1986). The best photographs, with clearly focused images, were selected for analysis.

Some data are also presented from a sample of *Lytechinus* spermatozoa reactivated at lower MgATP concentrations, using conditions similar to those reported previously (Brokaw, 1989*a*), and photographed with 12 flashes per second.

Data Analysis

The photographic negatives were scanned with a digitizing camera and the images were analyzed by computerized methods described previously (Brokaw, 1990), with the centerline of the flagellum modeled by a connected series of 0.5-μm straight segments. For each image, these methods provide values of bead position along the length of the flagellum, i.e., the distance from the basal end of the flagellum measured along the centerline of the flagellum to a point that is the projection of the bead position onto the centerline of the flagellum. Most of the images described here as beads are likely to be aggregates of several 40-nm gold beads. Since the apparent center of a bead can be distorted if its image intensity distribution is influenced by the presence of a nearby bead, the analysis program did not attempt to make any measurements of beads that were separated by distances of <0.5 μm. In addition, the angular orientation of the flagellum, relative to the head axis, at the position of each bead is determined.

Some flagellar bending waves can be described as sine-generated curves, in which curvature and shear angle are sinusoidal functions of length measured along the flagellum (Brokaw et al., 1970; Silvester and Holwill, 1972; Eshel and Brokaw, 1988). For such waves, plots of shear angle versus time should also be sinusoidal, and this representation is a useful approximation even for waves that are not exactly sine generated (Eshel and Brokaw, 1987). Time series obtained from the measurements of bead position and angular orientation of the flagellum have therefore been fitted with sinusoidal functions for the purposes of this analysis. For each pair of beads analyzed, the measurements of shear angle at both bead locations are fitted, using a nonlinear least-squares fit with seven parameters, to obtain a common value for the frequency of oscillation, and individual values for amplitude, phase, and mean angle at each bead location. This frequency is then used for a three-parameter fit to the data for the distance between the two beads, to obtain amplitude, phase, and mean separation.

The position, S_1, of a bead, projected onto the centerline of the flagellum, is therefore assumed to be

$$S_1 = S_{10} + D_1B_1 \sin(\omega t). \quad (1)$$

D_1 is the distance in the plane of bending from the centerline of the flagellum to the doublet microtubule on which the bead is riding. B_1 is the amplitude of oscillatory sliding of the doublet microtubule, measured in angular units, around the point S_{10} on the centerline of the flagellum. The angular frequency, ω, is equal to $2\pi f$, where f is the frequency of oscillation of the flagellum. Measurements of S_1 relative to the sperm head have not proven to be accurate enough to be used as the primary source of information about D_1. Greater accuracy is achieved by measuring the distance, S_2-S_1, between two beads on the flagellum:

$$S_2 - S_1 = S_{210} + D_2B_2 \sin(\omega t - \gamma) - D_1B_1 \sin(\omega t), \quad (2)$$

where γ is the phase difference between the shear angle oscillations at S_{20} and S_{10}, and S_{210} represents the constant distance $S_{20}-S_{10}$. Note that even in the case where two beads are located on the same doublet, so that $D_1 = D_2$, an oscillation in $S_2 - S_1$ can arise from the phase difference between the bead oscillations at S_{20} and S_{10}. An extreme example of this situation is illustrated in Fig. 8.

The shear angle, A_1, measured at the position of bead 1 will be given approximately by

$$A_1 = A_{10} + B_1 \sin(\omega t). \quad (3)$$

This is only approximate because the angles are measured at the position of the bead, S_1, and not at the fixed position, S_{10}. In an extreme case, if $D_1B_1 = 200$ nm, and the wavelength of the bending waves at the position of the bead is 20 μm, there will be an error oscillation with an amplitude of 0.2/20 = 0.01 cycles, or 0.063 rad, added to ωt in Eq. 3. This error is considered to be negligible in the following analysis, and initial estimates for B_1 are obtained from measured values of angle, A_1, using Eq. 3.

Fitting the measured values of $S_2 - S_1$ gives values for amplitude, B_3, and phase angle, α, from

$$S_2 - S_1 = S_{210} + B_3 \sin(\omega t - \alpha). \quad (4)$$

From Eqs. 2 and 4,

$$D_2 = (B_3/B_2)[\sin(\alpha)/\sin(\gamma)], \quad (5)$$
$$D_1 = -(B_3/B_1)[\sin(\gamma - \alpha)/\sin(\gamma)]. \quad (6)$$

B_3 can be determined from the fitting of $S_2 - S_1$ with greater accuracy than the phase angle, α, and γ is more accurately determined than α. Therefore, since

$$D_2 - D_1 = B_3 (B_1 \sin[\alpha] + B_2 \sin[\gamma - \alpha])/(B_1B_2 \sin[\gamma]), \quad (7)$$

and B_1 and B_2 for a pair of adjacent beads will usually have similar values, the doublet separation, $D_2 - D_1$, can be calculated more accurately than the individual values of D_2 and D_1.

An alternative to fitting $S_2 - S_1$ with Eq. 4 is determining the slopes of $S_2 - S_1$ vs. A_1 and A_2. The slope of $S_2 - S_1$ vs. A_1 should measure the por-

tion of $S_2 - S_1$ that is in phase with A_1, that is, in phase with $\sin(\omega t)$, and from Eq. 2 the slope will therefore be

$$\text{slope}_1 = D_2B_2\cos(\gamma)/B_1 - D_1. \quad (8)$$

Similarly, the slope of $S_2 - S_1$ vs. A_2 will be

$$\text{slope}_2 = -D_1B_1\cos(\gamma)/B_2 + D_2. \quad (9)$$

Therefore,

$$D_1 = -[\text{slope}_1 - \text{slope}_2\, B_2\cos(\gamma)/B_1]/[1 - \cos^2(\gamma)], \quad (10)$$

$$D_2 = [\text{slope}_2 - \text{slope}_1\, B_1\cos(\gamma)/B_2]/[1 - \cos^2(\gamma)], \quad (11)$$

$$D_2 - D_1 = [\text{slope}_1 + \text{slope}_2 - \cos(\gamma)[B_2\text{slope}_2/B_1 + B_1\text{slope}_1/B_2]/[1 - \cos^2(\gamma)]. \quad (12)$$

For very small values of γ, $B_1 \rightarrow B_2$, and $D_2 - D_2 \rightarrow (\text{slope}_1 + \text{slope}_2)/(1 + \cos[\gamma]) \rightarrow (\text{slope}_1 + \text{slope}_2)/2$. However, the individual values for D_1 and D_2 depend on the small difference between the nearly equal values of slope_1 and slope_2, so that much greater precision is required in the measurements of the slopes to obtain individual values for D_1 and D_2, as opposed to the sum $D_2 - D_1$. When the phase difference, γ, approaches π rad, the denominators in Eqs. 7 and 12 become small, and large errors in the results can be obtained if the data are imprecise. It is therefore prudent to limit the calculations to cases where the phase difference is not much greater than $\pi/2$ rad. Since the typical bending wave lengths for sea urchin spermatozoa are 30–40 μm, this means that the beads should not be separated by $>\sim 8$ μm.

After values for $D_2 - D_1$, D_1, and D_2 are obtained in this manner, the calculations can be repeated iteratively, replacing the approximate Eq. 3 with

$$A_1 = A_{10} + B_1\sin[\omega t - B_1D_1\gamma\sin(\omega t)/S_{210}]. \quad (13)$$

However, in all of the cases that were examined, the values of $D_2 - D_1$ were not significantly modified by this iterative recalculation (at most a change of 1 nm).

There are therefore two independent ways to fit the data and obtain the doublet separation, $D_2 - D_1$, one using B_3 and α, the other using slope_1 and slope_2. Both methods have been used routinely to calculate doublet separation, and the mean value has been used. In any cases where the two values obtained for the doublet separation did not agree closely, the analysis has been carefully examined for errors caused by inaccuracies in determining γ or α, and in a few cases the limiting value for $\gamma = 0$ has been used instead. Both procedures can in principle also yield independent values for D_1 and D_2, but only if the data are very precise.

Calculation of Theoretical Distributions

The doublet microtubules to which the measured beads are attached are not known. Interpretation of the doublet separations requires comparison of the distribution of measured doublet separations with the distribution expected from random attachment of beads to the outer doublet microtubules. In the simplest case, the expected distribution contains 81 values given by

$$\text{doublet separation/diameter} = \{\cos[2\pi(n - 1)/9] - \cos[2\pi(m - 1)/9]\}/2, \quad (14)$$

where n and m take on all possible values from 1 to 9 (Brokaw, 1989*a*). The diameter is the diameter of a circle passing through the neutral surface of each outer doublet, that is, the surface that undergoes no longitudinal compression or extension when the doublet bends. By measuring 81 values of doublet separation, the distribution of values given by Eq. 14 can be directly compared with the measured values (Brokaw, 1989*a*). Absolute values for both the theoretical and measured doublet separations are used in this comparison. If the number of measured values, n, is not equal to 81, an appropriate distribution can be obtained by a Monte Carlo simulation, in which n values are chosen at random from the 81 values given by Eq. 14, and the average of a large number of simulated distributions is used for comparison with the measured values.

Equation (14) is too simple, because it does not take into account several factors that sill tend to smooth the distribution. For the analyses in this paper, theoretical distributions have been obtained by Monte Carlo simulations, averaging 400 distributions obtained by selecting n values at random using the following equation:

$$\text{doublet separation/diameter} = \{1 + FV_1\}\{\cos[2\pi(n - 1)/9 + V_2] - \cos[2\pi(\text{m} - 1)/9 + V_2]\} + V_1)/2. \quad (15)$$

To obtain each value of doublet separation, a random variable is used to select an integer from the range 1 to 81, and values of n and m are then found such that the selected integer is equal to $9n + m$. V_1 is a random variable chosen from a Gaussian curve for a normal distribution. Its purpose is to incorporate into the theoretical distribution the effects of errors in measurement of the values of doublet separation and random variations in diameter in the population sampled. The standard deviation for this distribution, and the factor F, were determined empirically. F was determined by examining the relationship between the standard errors calculated for the slopes of the linear regressions of bead separation on shear angle and the values of the slopes. The values chosen were 0.25 for the *Ciona* sperm sample and 0.5 for the *Lytechinus* sperm sample. Values used for the standard deviation of V_1 were 0.08 for the *Ciona* sperm sample and 0.1 for the *Lytechinus* sperm sample. V_2 is a random variable chosen from a uniform distribution between 0 and $\pi/9$ rad. A value of $V_2 = 0$ corresponds to the assumptions that each bead is attached to just one outer doublet microtubule and the bending plane passes through doublet 1 and between doublets 5 and 6. A value of $V_2 = \pi/9$ corresponds to the assumption that each bead attaches to two adjacent microtubules, with the same bending plane. The uniform distribution allows for the uncertainty in how beads attach to the doublets and uncertainty in the exact position of the bending plane. Both V_1 and V_2 smooth the distribution. V_2 has very little effect on the shape of the distribution, while V_1 extends the tail of the distribution at high values of doublet separation.

After calculating the distribution, the value of diameter can be adjusted to give the minimum root mean square (RMS)[1] difference between the distribution and the measured values. This is done by sorting each distribution into increasing order of absolute values, and comparing the nth largest measured value with the nth largest calculated value, etc. Since this sorting of n values removes n-1 degrees of freedom from the distribution, the residual RMS difference between the measured and calculated values is interpreted as a standard error for the estimate of the diameter.

Results

Examples of Analyses of Bead Pairs on Individual Spermatozoa

One *Ciona* spermatozoon was chosen as an example to illustrate the methods used for analysis of bead movements and the character of the data that were obtained. Fig. 3 shows examples of computer monitor displays of two images of this spermatozoon, chosen to show the extremes of bead movement between the second and third beads on the flagellum (counting from the sperm head). In principle, the motion of each bead could be analyzed individually, using the measurements of its position relative to the sperm head. In practice, this has not been sufficiently accurate, and better information has been obtained by analyzing the relative motion of two beads separated by distances of no more than 8 μm. The eight beads that were measured on the flagellum shown in Fig. 3 provide five pairs of beads that can be analyzed for relative sliding motions, with mean separations between the beads of each pair ranging from 1.1 to 3.5 μm. Five multiple-flash photographs of this spermatozoon, each containing $\sim$50 images, were available for analysis. In the first three photographs, the flagellum was beating with a stable frequency of 26.2 Hz. Between the third and fourth photographs, the frequency dropped to 24.8 Hz, and the fourth bead disappeared from the flagellum. The combined results for analysis of this spermatozoon are summarized in Table I, with standard deviations for the sample of five photographs. For bead pair 4–5, only the results from the first three photographs are given. Bead pair 2–3 of this spermatozoon showed the largest amplitude of oscillation of bead separation (B_3 = 289 nm) found in the *Ciona* sample. Results of the analysis of this bead pair, from one of the photographs, are shown in Figs. 4 and 5.

1. *Abbreviation used in this paper*: RMS, root mean square.

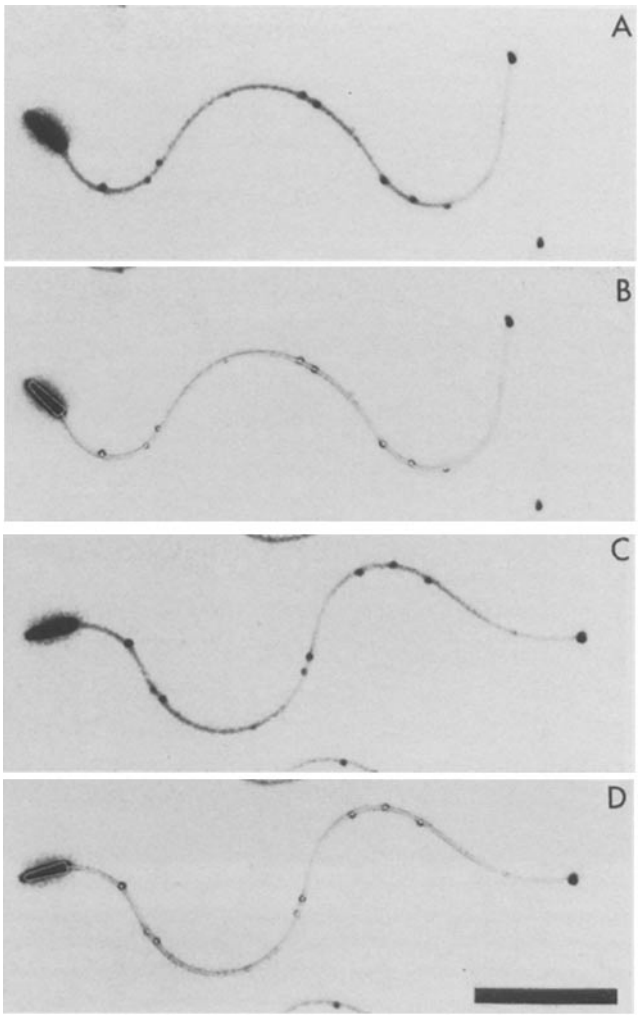

Figure 3. Portions of computer monitor displays of two images from a multiple-exposure photograph of a *Ciona* spermatozoon labeled with gold beads. *A* and *B* show image 33 and *C* and *D* show image 5, corresponding to the image numbers in Fig. 4. In *B* and *D*, the results of image analysis to locate the sperm head, the centerline of the flagellum, and the positions of eight beads are shown superimposed on the gray level displays of the images. Bar, 10 μm.

The upper panel of Fig. 4 shows the measured values of the distance between beads 2 and 3, referred to here as bead separation ($S_2 - S_1$), from 49 images in this photograph. The lower panels show the shear angles (A_1 and A_2) at the position of each bead, measured relative to the sperm head axis. These time series were fitted with sinusoidal functions, as described under Data Analysis, and the sinusoidal curves have been drawn in the figures. For the shear angle data, the amplitude and phase of oscillation of each shear angle are represented in Table I by the mean amplitude and the phase difference, γ, between the oscillations. The RMS error remaining after fitting the angles can arise from difference between the sinusoidal waveform that was fitted and a true nonsinusoidal flagellar waveform, from time variations in the behavior of the flagellum, and from errors in the measurements. The range of RMS errors obtained with this spermatozoon (0.08 to 0.10 rad) is at the low end of the range of values obtained with this *Ciona* sperm sample (mean 0.12 $\pm$ 0.03 rad [SD]). The sea urchin sperm sample typically gave larger RMS error values (0.17 $\pm$ 0.08 rad), probably because the beating of their flagella was less regular and a larger number of beat cycles was sampled. The small standard deviations for the amplitudes of shear angle oscillation and the phase difference, γ, also indicate that the beating of this sperm flagellum was very regular over the period covered by these five photographs, in spite of the change in frequency that was observed.

The measured values for the bead separations are typically noisier than the shear angle values; this is indicated by the larger values for the RMS error after fitting the bead separation oscillation, relative to the amplitude of oscillation (16 compared with 9%). The relative standard deviations for the bead separation amplitudes are also large compared to the standard deviations for the shear angle amplitudes.

Values for the doublet separation ($D_2 - D_1$), representing the separation between the two outer doublet microtubules marked by a particular pair of beads, were calculated from the amplitudes and phases of these sinusoidal oscillations using Eq. 7 and are given in Table I.

Fig. 5 presents the same results as plots of bead separation versus shear angle for each of the beads of pair 2–3. The results were analyzed by linear regression of bead separation on shear angle, since the apparent errors in the bead separation measurements are usually large relative to the apparent errors in shear angle. The linear regressions provide two values of slope that can be used to calculate the doublet separation ($D_2 - D_1$) by Eq. 12, and these results are also given in Table I. For these bead pairs, there is excellent agreement between the values of doublet separation calculated by the two methods. The linear regression analysis also provides estimates for the error in the calculated slopes, and the means of these values are also shown in Table I. However, an exact linear relationship between bead separation and shear angle can be expected only if the two oscillations are in phase, which can never be exactly true for both beads. For beads that are close together so that all of the phases are similar, such as the pair analyzed in Figs. 4 and 5, this effect is small compared with the scatter in the data. For beads that are farther apart, with substantial phase differences, the errors calculated for the slopes may overestimate the errors in the values of doublet separation. This appears to be the case for bead pairs 6–7 and 7–8 in this example, where the errors calculated for the slopes are larger than the standard deviations for the independent measurements of doublet separations obtained from each of the five multiple-exposure photographs. These standard deviations for the doublet separations probably provide the best indicator of the precision of the measurements of doublet separations.

Standard deviations for the doublet separations were also calculated from three computerized image analyses of the same image scans of one of these multiple-exposure photographs, using slightly different fitting parameters, and from analyses of three independent sets of image scans of the same photograph. In the first case, the average standard deviation was 20% of the average standard deviation obtained from analysis of the five multiple-exposure photographs. In the second case, the average standard deviation was 40% of the average standard deviation obtained from analysis of the five photographs. These comparisons indicate that little improve-

Table I. Analysis of Five Bead Pairs on a Ciona Spermatozoon: Means and SD Values from Measurements of Five Multiple-Exposure Photographs

Parameter	Beads 1-2	2-3	4-5	6-7	7-8
Distance from base of flagellum (μm)	5.8	8.2	21.9	30.6	33.4
Mean separation between beads (μm)	3.5	1.1	1.2	2.5	2.6
Mean amplitude of angle oscillation ($B_1 + B_2$)/2(*rad*)	1.30 ± 0.01	1.44 ± 0.01	0.83 ± 0.02	0.94 ± 0.04	1.14 ± 0.03
RMS error after fitting angles (*rad*)	0.08 ± 0.01	0.09 ± 0.01	0.10 ± 0.02	0.09 ± 0.02	0.10 ± 0.02
Phase difference, γ, between angle oscillations (*rad*)	0.61 ± 0.03	0.17 ± 0.0	0.26 ± 0.01	0.58 ± 0.02	0.49 ± 0.01
Amplitude of bead separation oscillation, B_3 (*nm*)	−212 ± 11	289 ± 8	−63 ± 4	141 ± 11	−161 ± 3
RMS error after fitting bead separation oscillation (*nm*)	25 ± 3	24 ± 2	19 ± 1	22 ± 2	24 ± 3
Phase difference, α, between bead separation and angle at first bead (*rad*)	0.23 ± 0.03	0.08 ± 0.02	−0.14 ± 0.19	0.31 ± 0.03	0.15 ± 0.04
Doublet separation, D_2-D_1, from sinusoidal analysis (*nm*)	−177 ± 9	202 ± 6	−66 ± 14	157 ± 5	−152 ± 5
Doublet separation, D_2-D_1, from slope analysis (*nm*)	−176 ± 8	202 ± 6	−64 ± 16	157 ± 4	−152 ± 5
Standard error for slope (*nm*)	9.2 ± 0.7	4.9 ± 0.6	7.8 ± 1.0	8.7 ± 0.5	7.4 ± 0.6
D_1 (*nm*)	119 ± 11	−111 ± 24	−111 ± 55	−81 ± 8	109 ± 10
D_2 (*nm*)	−58 ± 8	91 ± 24	46 ± 69	76 ± 11	−42 ± 12

ment in precision is to be expected from any further refinement of the image analysis methods, and that taking more photographs is the best way to improve the results.

Fig. 6 shows curves for shear angle plotted as a function of position along the length of the flagellum, at 12 successive times in the beat cycle, obtained from analysis of 12 successive images on one of the photographs of the spermatozoon shown in Fig. 3. The curves in Fig. 6 *A* have been obtained directly from the fitting process, without any additional smoothing or adjustment, and show the shear angles measured relative to the axis of the sperm head. If these curves are interpreted as a description of the pattern of sliding between flagellar microtubules, they indicate that the amplitude of oscillatory sliding is not uniform along the length of the flagellum. Shear curves such as these for all of these *Ciona* sperm flagella consistently show a minimum in the amplitude of shear angle oscillation, between 25 and 30 μm from the basal end of the flagellum. In other work, it can be seen that the location of this minimum depends upon the wavelength of the bending waves. Examples with shorter

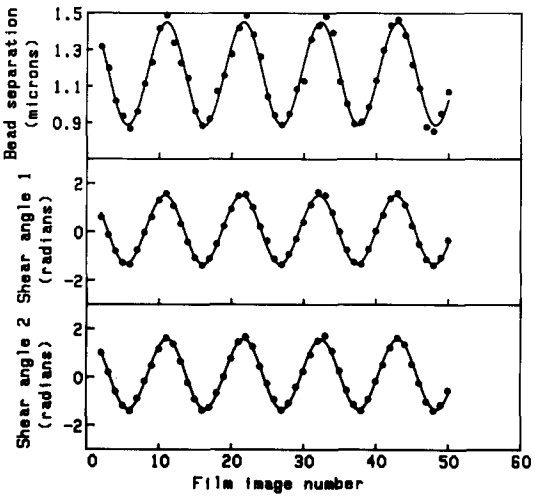

Figure 4. Measurements of bead separation and shear angle as a function of time for beads 2 and 3 on the flagellum in Fig. 3, fitted with sinusoidal functions. This spermatozoon was photographed at 280 images per s for ~0.2 s, and the photograph contained 49 usable images.

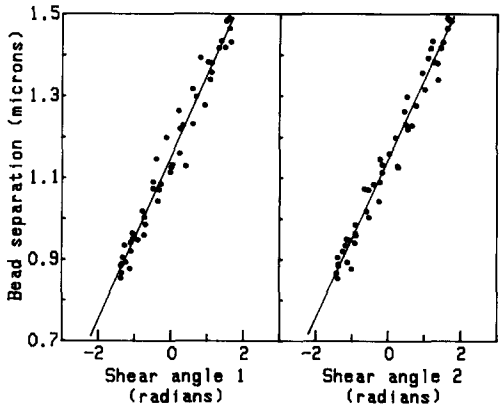

Figure 5. The data from Fig. 4 replotted to show the linear regression of bead separation on shear angle at each of the two beads. The slopes of the regression lines are 199 and 194 nm/rad, with standard errors of 5 nm/rad.

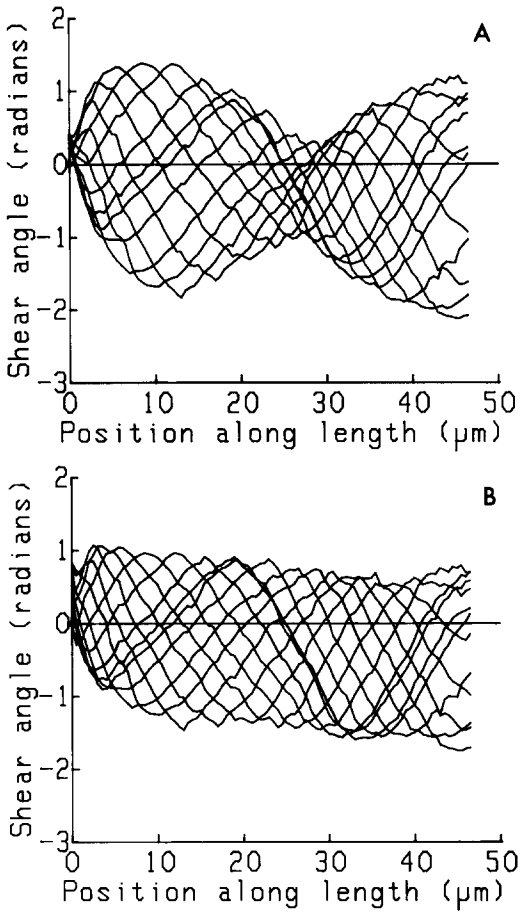

Figure 6. Plots of shear angle vs. position on the flagellum for 12 images covering one beat cycle of the *Ciona* spermatozoon shown in Fig. 3. In *A*, the shear angles are those measured relative to the head axis. In *B*, the shear angles have been modified by subtracting a sinusoidal oscillation in shear angle as a function of time, with amplitude and phase chosen to obtain a more uniform amplitude of shear angle oscillation along the length of the flagellum.

bending waves, clearly showing two minima and two maxima along the length of the flagellum, are shown by Gibbons (1981) and by Eshel and Brokaw (1987). This nonuniform sliding pattern can be resolved into a metachronous component, representing a wave of oscillatory sliding with constant amplitude along the length, and a synchronous component, by subtracting from the data a sinusoidal oscillation of shear angle with constant phase along the length of the flagellum. The frequency of this oscillation is the same as the flagellar beat frequency. The amplitude and phase of the oscillation to be subtracted can be determined by trial and error, until the result looks like the pattern in Fig. 6 *B*. In this particular case, the amplitude is 0.43 rad.

If an oscillation in bead separation is compared with the metachronal shear oscillation (Fig. 6 *B*), instead of the shear oscillation relative to the head (Fig. 6 *A*), different values of doublet separation, $D_2 - D_1$, may result. The values of doublet separation will be decreased in regions near the minima of shear oscillations in Fig. 6 *A*, and increased in regions near the maxima of shear oscillations. For example, for bead pair 2–3 in this example, the mean amplitude of shear angle oscillation is reduced from 1.44 to 1.04 rad, and the calculated doublet separation increases from 202 to 279 nm. Since the latter value is large compared to a reasonably expected value for the diameter of the axoneme, the pattern in Fig. 6 *A* could be concluded to be a more accurate description of sliding in the flagellum than Fig. 6 *B*.

Fig. 7 shows measurements of a pair of beads on a *Ciona* flagellum that provide an example of results indicating relatively small relative motion of a pair of beads. In this case, the sinusoidal analysis (Fig. 7 *A*) detects an oscillation in bead separation with an amplitude of −11 nm, with a residual RMS error of 28 nm. The slope analysis (Fig. 7 *B*) detects slopes of −5 and −6 nm/radian. The analysis results in a value of −6 nm for doublet separation, $D_2 - D_1$, but this value is not large compared to the errors. Fortunately, for interpretation of the results in this paper, it is sufficient to determine that the doublet separation is small, and not necessary to know whether it is significantly different from 0.

The example in Fig. 8 shows an apparent oscillation in separation between two beads that are widely separated (6.9 μm) along the length. This oscillation is not in phase with either of the angle oscillations, so that the regression plots show elliptical rather than linear patterns. This apparent oscillation in bead separation could therefore result from the phase difference between oscillations of two widely separated beads that are both located well to the same side of the flagellar centerline. In this example, the phase difference between the shear angle oscillations is 1.15 rad, and the phase of the bead separation oscillation is 1.93 rad ahead of the shear angle oscillation of the first bead of the pair. The bead separation oscillation could result if D_1 and D_2, the distances

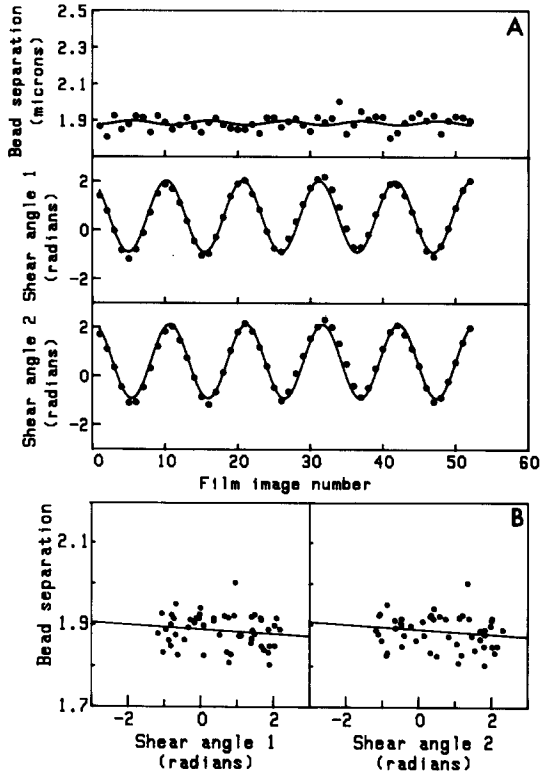

Figure 7. Bead separation and shear angle for a pair of beds on a *Ciona* sperm flagellum showing a very small oscillation in bead separation.

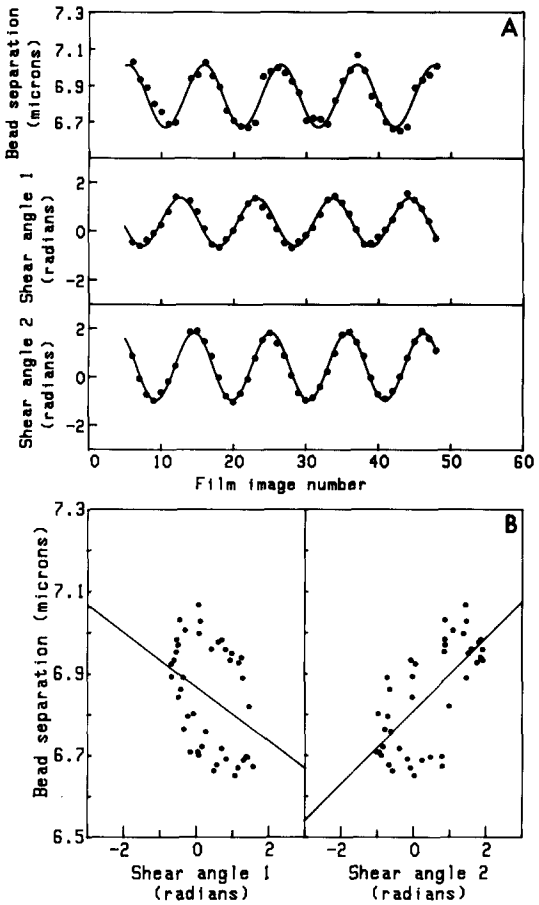

Figure 8. Bead separation and shear angle for a pair of beads on a *Ciona* sperm flagellum that are separated by a relatively large distance (~6.9 μm), showing an oscillation in bead separation that is out of phase with the shear angle oscillations.

between the labeled doublets and the flagellar centerline, have values of 136 and 128 nm, respectively; the value of $D_2 - D_1$ is then only −8 nm. Alternatively, some or all of an out of phase bead separation oscillation might result from changes in lengths of microtubules (cf. Brokaw, 1989*a*), and the analysis does not distinguish that possibility. In either case, only the portion of the oscillation that has the proper phase to result from microtubule sliding is relevant to the results of this paper, and that portion is represented by the doublet separation value of −8 nm.

Table II summarizes measurements obtained from five beads on a sea urchin sperm flagellum. Plots of shear angle vs. position for this flagellum show the same type of nonuniform shear angle amplitude as Fig. 6 *A*, with a minimum amplitude near 20 μm. The nonuniformity can be removed by subtracting from the shear angles a synchronous sinusoidal component with an amplitude of 0.38 rad at the frequency of 17.6 Hz determined from the analysis of the shear angle oscillations at the bead locations. In this case, the amplitude and phase for the synchronous component were determined by fitting a sinusoidal oscillation to measured values for the angular orientation of the head as a function of time.

The amplitudes of shear angle oscillation near the midregion of this flagellum obtained from measurements relative to the sperm head axis are relatively small, with a mean amplitude of 0.63 rad for the fourth and fifth bead. The value of doublet separation calculated from the measurements on beads 4 and 5 is 280 nm, much larger than reasonable values (< 200 nm) for the diameter of a sea urchin axoneme. After subtracting the head oscillation to obtain a metachronous sliding pattern with more nearly uniform amplitude, the mean amplitude of shear angle oscillation for this bead pair increases to 0.91 rad, and the calculated value of doublet separation for bead pair 4–5 is reduced to 172 nm, which is now a reasonable value. The measurements on this sea urchin sperm flagellum therefore indicate that a more reasonable sliding pattern is obtained by subtracting the head oscillation from the angles measured relative to the head axis. Sliding calculated as the angle relative to the sperm head axis is therefore inaccurate in this case. The same conclusion could be reached from another sea urchin sperm flagellum, which had a pair of beads giving a doublet separation of −402 nm before adjustment and −151 nm after adjustment.

Another important feature of the results is indicated in Tables I and II. Although in many of these cases the doublet separations for adjacent bead pairs are relatively large, they alternate in sign so that no two (or more) adjacent values of doublet separation add up to values that are unreasonably large compared to the diameter of the axoneme. This was true of all the bead pairs that were measured. It provides strong evidence that the measured values are really measuring the doublet separation, and are not just noise.

Information Provided by Individual Beads

In principle, even if a bead is located too far from the sperm head for accurate measurement of its position relative to the sperm head, the distance between a doublet marked with a bead and the centerline of the flagellum can be calculated from the analysis of the relative motion of two beads, if the phase of the oscillation in bead separation can be accurately measured. For a particular pair of beads, these individual values are indicated by D_1 and D_2, and can be calculated from Eqs. 5 and 6. However, as can be seen in Table I, the measured values for the phase angle for the bead separation oscillation, which is given in terms of α, the phase difference between the bead separation oscillation and the shear angle oscillation for the first bead of the pair, have relatively larger standard deviations than the oscillation amplitudes or the phase difference, γ, between the angle oscillations.

Table I shows individual values of D_1 and D_2 which are means of the values calculated from the sinusoidal analysis (Eqs. 5 and 6) and the slope analysis (Eqs. 10 and 11). As expected, these values usually have much larger relative standard deviations than the doublet separation $D_2 - D_1$. In this example, bead 1 was about 4 μm from the sperm head, and measurements of this distance on the 49 images in the photograph from which Figs. 3–5 were taken gave reasonable results. The time series for these measurements indicated an amplitude of oscillatory sliding of 173 nm for bead 1, with an RMS error of 30 nm. However, the apparent phase of this oscillatory sliding was 0.3 rad behind the oscillation of shear angle at bead 1. If this phase difference is considered to result from measurement errors, and is ignored, D_1 should be equal to the slope of the regression of bead movement on shear angle (126 nm/rad), and also to the ratio of the amplitudes of oscillatory sliding and shear angle (134

Table II. Analysis of Four Adjacent Bead Pairs on a Lytechinus Spermatozoon

Parameter	Beads 1-2	2-3	3-4	4-5
Distance from base of flagellum (μm)	10.8	14.0	15.0	17.7
Mean separation between beads (μm)	5.7	0.7	1.1	4.3
Mean amplitude of angle oscillation $(B_1 + B_2)/2$ (*rad*)	1.13	0.85	0.77	0.63
Phase difference, γ, between angle oscillations (*rad*)	0.97	0.11	0.20	1.04
Amplitude of bead separation oscillation, B_3 (*nm*)	−112	141	−82	145
Phase difference, α, between bead separation and angle at first bead of pair (*rad*):	0.94	0.55	0.58	0.79
Doublet separation, D_2-D_1 (*nm*)	−121	163	−113	280
Standard error for slope (*nm*)	13	15	11	18
D_1 (*nm*)	2	640	−174	−40
D_2 (*nm*)	−118	824	−296	240
Adjusted data: synchronous sliding eliminated by subtraction of head oscillation				
Amplitude of angle oscillation (*rad*)	1.01	0.95	0.94	0.91
γ (*rad*)	1.19	0.11	0.19	0.73
α (*rad*)	0.76	0.14	0.20	0.52
D_2-D_1 (*nm*)	−130	148	−88	172
D_1 (*nm*)	49	15	15	−51
D_2 (*nm*)	−81	163	−73	121

nm/rad); in this case the average value of 130 nm for D_1 agrees reasonably well with the value of 119 nm calculated from analysis of the relative movements of beads 1 and 2 (Table I).

On the other hand, the value in Table I for D_2 (for bead 2) calculated from analysis of the relative movements of beads 1 and 2 should be the same as the value for D_1 (for bead 2) calculated from analysis of the relative movements of beads 2 and 3, but these values are −58 and −111 nm, respectively. Similarly, D_2 for bead pair 6–7 (76 nm) should be the same as D_1 for bead pair 7–8 (109 nm). These values do not agree well, and differences of this magnitude or greater were typical. Therefore, these individual values for doublet position relative to the centerline of the flagellum have not been considered to be very useful, except in a few special cases.

In the case of the sea urchin sperm flagellum in Table II, bead pairs 2–3 and 3–4 show a bead separation oscillation that is significantly out of phase with the shear angle oscillations. With these phase relationships, the measured shear oscillation can only be obtained if the beads are riding on doublets that are far from the centerline of the flagellum, as indicated by the values of 640 nm for D_1 and 824 nm for D_2 for bead pair 2–3 (Table II). This is an unreasonable conclusion. However, after adjustment by removal of the head oscillation, in the lower part of Table II, the phases of the shear angle oscillations and the bead separation oscillation are close together, and the head separation oscillation can be obtained with reasonable values for D_1 and D_2. Another consequence of the differences in phase between the shear angle oscillations and the bead separation oscillations is that the two values of D_n calculated for each of the beads 2, 3, and 4 by considering the bead pair separations are grossly different before adjustment by removal of the head oscillation and somewhat more similar after removal of the head oscillation.

Several other sea urchin sperm flagella had series of beads that showed inconsistent phase relationships before adjustment and more reasonable phase relationships after adjustment by subtraction of a synchronous sliding component. These examples therefore provide some additional evidence that the adjusted shear angle curves provide a more accurate description of sliding in sea urchin sperm flagella.

Analysis of the Full Samples of Bead Pairs

Fig. 9 shows results for 234 bead pairs measured on the sample of 69 *Ciona* spermatozoa, selected from 121 spermatozoa that were photographed. These results are all presented as distributions along the length of the flagellum. Means were calculated for the values in eight bins, corresponding to 6-μm intervals along the length, and plotted at the mean value of position for the values in each bin. These means are connected by a line drawn in each graph. The spermatozoa in this sample had a mean beat frequency of 26.1 ± 1.5 Hz (SD). The mean amplitude of the "oscillatory synchronous sliding" component that was subtracted to obtain a uniform distribution of amplitudes of angular oscillation along the length was 0.35 ± 0.05 rad. The beads in this sample were separated by mean distances (S_{210}) of <8 μm; and only three pairs were separated by >6.5 μm. The values of S_{210} had a mean of 3.0 μm, standard deviation of 1.6 μm, and median of 2.8 μm.

Each point in Fig. 9 *A* is the mean of the two amplitudes of oscillation of shear angle, measured relative to the centerline of the sperm head, for each bead pair. The distribution shows a pronounced minimum at ~25 μm along the length,

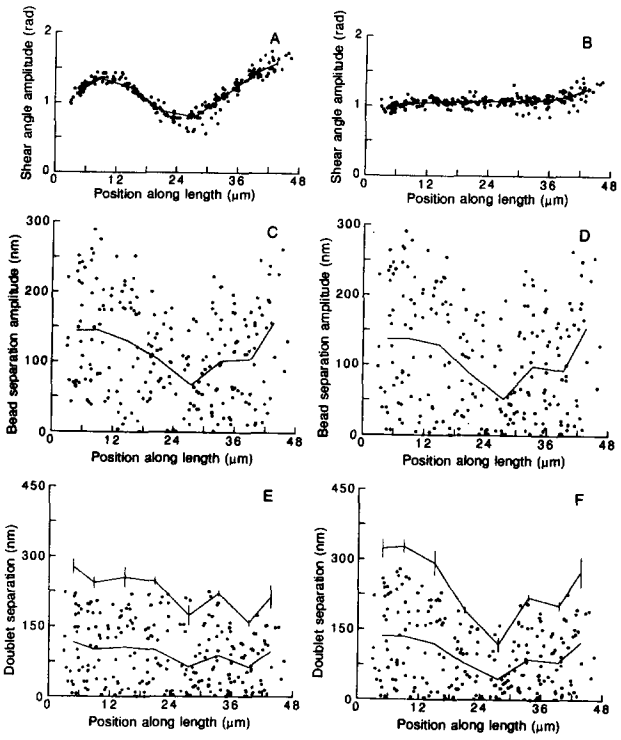

Figure 9. Distribution of measurements along the length of the flagellum for the 234 bead pairs of the *Ciona* sperm sample. (*A*) Measurements of amplitude of shear angle oscillation. (*B*) Measurements of amplitude of shear angle oscillation after adjustment by subtracting a synchronous oscillation to obtain uniform amplitudes along the length, as shown in Fig. 6 *B*. (*C*) Measurements of amplitude of bead separation oscillation. (*D*) Corrected values for the amplitude of bead separation oscillation, obtained by calculating doublet separation and multiplying by the shear angle amplitude. (*E*) Calculated values of doublet separation, D_2-D_1, using the shear angles in *A*. (*F*) Calculated values of doublet separation, using the adjusted shear angles in *B*. Lines are drawn through the mean values for each 6-μm bin, positioned at the mean of the values of position for the beads in each bin. *E* and *F* also contain lines connecting values of axonemal diameter calculated from the distribution of the values of doublet separation in each bin, and the standard error estimates for these values of diameter are shown.

corresponding to the reduced amplitudes of shear angle oscillation at that position seen in the patterns obtained from individual sperm flagella, as in Fig. 6 *A*. Fig. 9 *B* shows the amplitude values obtained after subtracting an oscillatory synchronous sliding component from each flagellum. Fig. 9 *C* shows the values obtained for B_3, the amplitude of oscillation of the distance between the two beads of each pair, measured along the centerline of the flagellum. These values obviously show much greater scatter everywhere on the flagellum, because the oscillation of bead separation is the product of the shear angle oscillation and the doublet separation, which can vary between 0 and the axonemal diameter. Nevertheless, this figure clearly reveals a nonuniform distribution of values along the length of the flagellum, with a minimum at about the same position as the minimum of the shear angle distribution shown in Fig. 9 *A*. However, these values of amplitude are not appropriate for comparison with the shear angles, because they include the effects of phase differences between the oscillations of the two beads in a pair, which can be as extreme as shown by the example in Fig. 8. To correct these values, true amplitudes of bead separation oscillation that represent sliding between the beads are shown in Fig. 9 *D*, obtained by calculating doublet separation, $D_2 - D_1$, and multiplying by the mean amplitude of shear angle oscillation for each bead pair. This corrected distribution also shows a minimum at ~26 μm from the base of the flagellum, corresponding to the minimum in shear angle amplitudes seen in Fig. 9 *A*.

Fig. 9 *E* shows the calculated values of doublet separation for each bead pair. The lower line is drawn through the means for each bin; no standard errors are shown because these values are not drawn from a normal distribution. The upper curve shows the values calculated for the diameter of the axoneme that gives the best fit of Eq. 15 to the distribution of values in each bin. The standard error estimates for these values of diameter are also shown. Fig. 9 *F* shows in the same manner the values of doublet separation calculated by using the modified shear angle amplitudes of Fig. 9 *B*, with the synchronous sliding removed. Since the amplitudes in Fig. 9 *B* are relatively constant, Fig. 9 *F* shows a minimum corresponding to the minimum seen in Fig. 6 *D*. Since we expect a distribution that shows a constant axonemal diameter, independent of position along the flagellum, Fig. 9 *E* appears to be more realistic than Fig. 9 *F*, and the shear angle amplitudes of Fig. 9 *A* are therefore more correct than those in Fig. 9 *B*.

Fig. 10 uses the same format as Fig. 9 to show results for 330 bead pairs measured on the sample of 76 *Lytechinus* spermatozoa, selected from 242 spermatozoa that were pho-

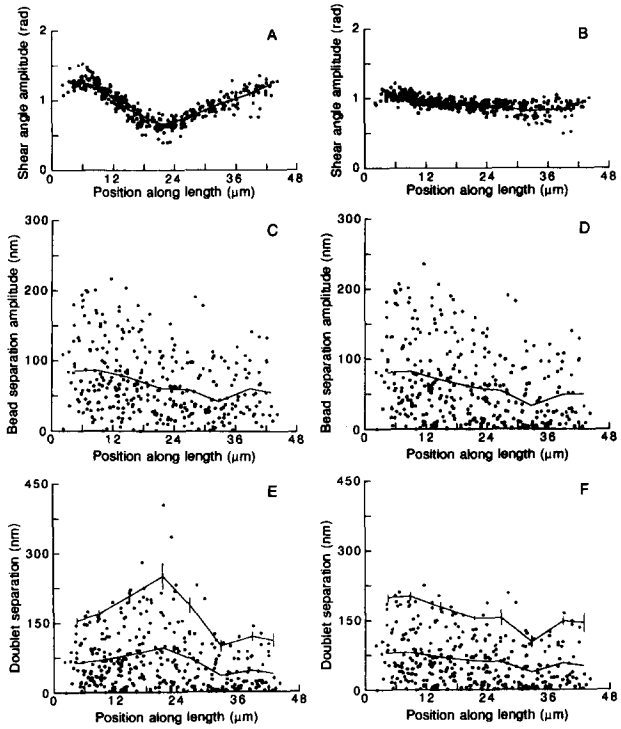

Figure 10. Distribution of measurements along the flagellum for the 330 bead pairs of the *Lytechinus* sperm sample. See legend to Fig. 9 for explanations.

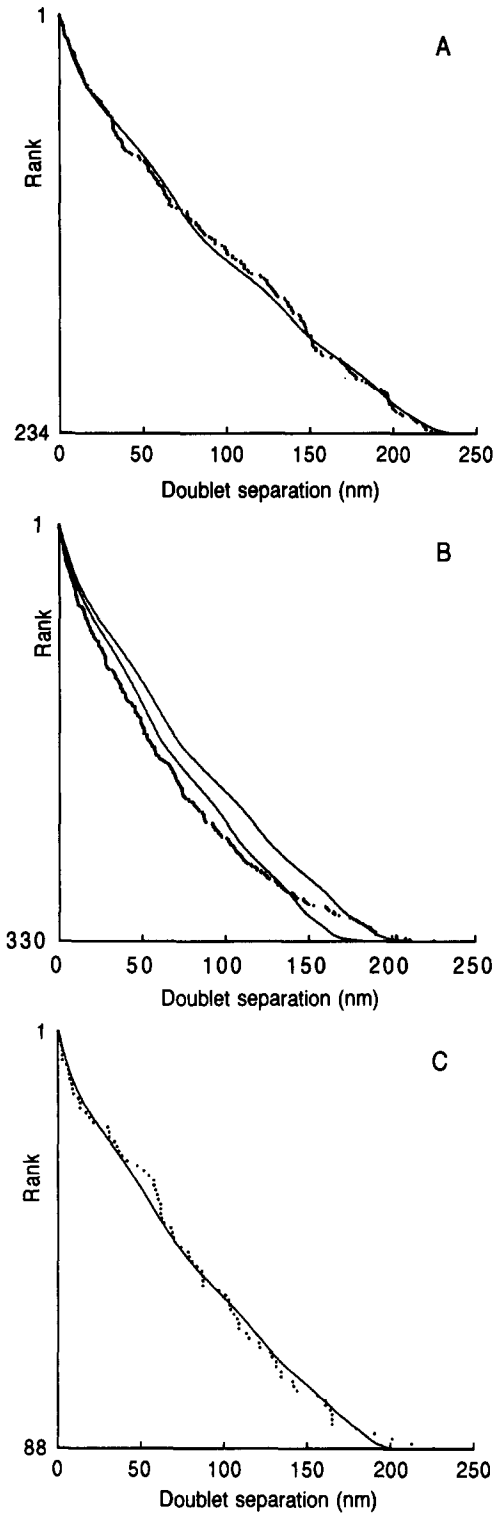

Figure 11. Absolute values of doublet separation, arranged in ascending order from top to bottom of the plot, are shown by small dots. The lines are obtained from Monte Carlo simulation of the theoretical distributions for random attachment of beads to doublets, given by Eq. 15 in the text. Data from the *Ciona* sperm sample are shown in *A*; the diameter for the theoretical distribution is 227 nm. Data from the *Lytechinus* sperm sample at high MgATP concentration are shown in *B*; the diameters for the two theoretical distribution curves are 167 and 194 nm. Data from a *Lytechinus* sperm sample at low MgATP concentration are shown in *C*; the diameter for the theoretical distribution curve is 196 nm.

tographed. The spermatozoa in this sample had a mean beat frequency of 18.0 ± 1.1 Hz (SD). The mean amplitude of the "oscillatory synchronous sliding" component that gave the most uniform amplitudes of angular oscillation along the length was 0.29 ± 0.09 rad. Measurements were also made of the amplitude of oscillation of the sperm head, yielding a mean of 0.29 ± 0.07 rad. The values of angular amplitude obtained by these two methods were well correlated, with $r = 0.86$. The beads in this sample were also separated by mean distances (S_{210}) of <8 μm; and only five pairs were separated by >6.5 μm. The values of S_{210} had a mean of 2.8 μm, standard deviation of 1.5 μm, and median of 2.6 μm.

The amplitudes of oscillation of bead separation, B_3, from the *Lytechinus* sperm sample are shown in Figs. 10 *C* (uncorrected) and 10 *D* (corrected to represent sliding only). In this case, there is no minimum at the position of the minimum in the amplitudes of angular oscillations at ~23 μm from the base (Fig. 10 *A*). Instead, there is a large maximum in the distribution of values of doublet separation, $D_2 - D_1$, at this position, as shown in Fig. 10 *E*. As shown in Fig. 10 *F*, this maximum is eliminated by calculating the values of doublet separation with the modified angular amplitudes of Fig. 10 *B*, indicating that these modified shear angle amplitudes more accurately describe the sliding that is occurring in these flagella.

Fig. 11 presents a comparison of the full distributions of measured doublet separation values, $D_2 - D_1$, with the distributions expected if the beads attach randomly to outer doublets, calculated from Eq. 15. For the *Ciona* spermatozoa (Fig. 11 *A*), the measured doublet separations shown are the ones shown in Fig. 9 *E* that were calculated from the measurements of shear angle relative to the axis of the sperm head. For the *Lytechinus* spermatozoa (Fig. 11 *B*), the measured doublet separations shown are the ones shown in Fig. 10 *F*, calculated from the modified amplitudes of angular oscillation in Fig. 10 *B*, obtained by subtracting a synchronous sliding component. These choices were made to avoid distortion of the distribution by variations along the length of the flagellum, shown by the plots in Figs. 9 *F* or 10 *E*. For the plots in Fig. 11, the values are sorted and plotted in ascending order of absolute value of doublet separation, from the top to the bottom of the graph. The *Ciona* data are fitted best by the theoretical distribution when it is calculated with a diameter of 227 nm, using a value of 0.08 for the standard deviation of the random component, V_1; there is a residual RMS error of 4.7 nm. The *Lytechinus* data do not match the shape of the theoretical distribution well. Fig. 11 *B* shows two theoretical distribution curves, corresponding to the same distribution (with an SD of 0.10 for V_1) and two different values of diameter. A diameter of 167 nm gave the best overall fit, with a residual RMS error of 9.9 nm. A diameter of 194 nm was required to adequately fit the largest measured values of doublet separation; this had a residual RMS error of 16.7 nm.

Fig. 11 *C* shows results for a smaller sample (88 bead pairs) from 17 *Lytechinus* spermatozoa reactivated under conditions similar to earlier work (Brokaw, 1989*a*), at a mean beat frequency of 0.8 Hz. The theoretical distribution, with an SD for V_1 of 0.08, gives a good fit with a diameter of 196 nm and a residual RMS error of 5.8 nm. These spermatozoa were selected to have low head oscillation amplitudes (0.08 ± 0.03 rad). There was little difference between

the distributions obtained with or without (Fig. 11 *C*) adjustment to obtain uniform shear angle amplitudes.

Plots similar to Figs. 9–11 were prepared for data subsets obtained by retaining bead pairs with values <5 μm for the mean separation, S_{210}, and values <40 nm for the RMS error remaining after fitting the bead separation data with a sinusoidal function. 183 pairs were retained in the *Ciona* subset and 263 pairs were retained in the *Lytechinus* subset. The conclusions from examining these subsets were identical to those from the full data sets.

Discussion

The major conclusion of this work is shown in Figs. 9 and 10. With *Ciona* spermatozoa, the patterns of sliding revealed by measuring shear angles relative to the sperm head axis, as in Fig. 6 *A*, are confirmed by the agreement between the distributions of shear angle oscillation amplitudes (Fig. 9 *A*) and direct measurements of sliding using beads as markers of the movements of outer doublet microtubules (Fig. 9 *D*). With the *Lytechinus* sperm sample, the direct measurements of sliding do not agree with the values calculated by measuring angles and therefore demonstrate that values of sliding calculated from angles measured relative to the sperm head axis can be seriously inaccurate. Sliding amplitudes that are more consistent with direct measurements of sliding (Fig. 10 *D*) are obtained by removing a synchronous component from the shear angles measured relative to the head axis (Fig. 10 *B*). Before trying to interpret this conclusion, the validity of the measurements leading to it are discussed below.

Tests of the Validity of the Measurements

Some of the bead pairs, such as the 2-3 bead pair of Fig. 3, reveal relatively large and clear changes in bead separation that can be confirmed by direct measurements, projecting the films on a screen and using a ruler to measure distances between the beads. Although such measurements (not presented here) are not individually precise, they demonstrate that there is no large (e.g., ± 20%) systematic difference between these direct measurements and the measurements made by computerized image analysis.

If the centerline determined by analysis of a flagellar image is not as smooth as the true centerline of the flagellum, it will be longer, leading to an overestimation of distances between beads. This effect is very small. Typical values for the noise in determining the curvature of the flagellum by the image analysis method used here are ~0.1 rad/μm (Brokaw, 1990, Fig. 4). This would correspond, in the worst case, to approximation of a straight line by a "sawtooth" wave made of 0.5-μm segments, with alternating slopes of + or −0.025 rad. The ratio between the true length on the straight line, and the length of each 0.5-μm segment, would be equal to cosine (0.025 rad) or 0.9997.

There may also be errors in approximating the centerline of a curved flagellum with a series of straight segments. In a region of the flagellum with a maximal curvature of 0.2 rad/μm that is approximated by 0.5-μm segments that are tangent to the curve, the true arc length will be 0.4996 μm per segment. If the end points of the segments are on the curve, the true arc length will be 0.5002 μm per segment. The fitting process should place the segments intermediate between these two extremes, and the errors will be negligible. Larger errors could result if the fitting process consistently places the segments either outside of or inside of the centerline in curved regions. However, with beads that are no more than 2 to 3 μm apart, the most significant measurement are made when the region between the beads is nearly straight, and will be unaffected by such errors.

Large bead aggregates attached to an outer doublet microtubule at one point might be tilted by viscous drag as the flagellum moves through the solution, so that the center of the image of the aggregate does not identify a consistent position on the outer doublet to which it is attached. However, two beads that are close together, even if on opposite sides of a flagellum, will be subjected to similar viscous drag forces and will tend to shift in the same direction, with little change in the distance between their centers. If the beads are farther apart, the tilt effects will be out of phase, and should not contribute to the in phase measurements that are interpreted here as measures of doublet microtubule sliding. If one bead of a pair is able to tilt, while the other does not, the situation may be different, but as long as this distinction between the two beads occurs randomly, this effect will not introduce a systematic error.

The comparison of direct measurements of sliding with sliding calculated from shear angles would be straightforward if it were possible to identify the outer doublet microtubules to which a given pair of beads is attached. Without this information, the comparison depends upon the assumption of random attachment of beads to microtubules, so that the resulting distribution of doublet separations is predictable. The data provide several tests of this assumption.

One test is provided by comparing the shape of the distribution of values of doublet separation calculated from measurements of sliding and shear angle with the shape of the distribution expected from uniform, random, attachment of beads to the exposed outer doublet microtubules of an axoneme. This comparison is illustrated in Fig. 11, and in Fig. 4 of Brokaw (1989*a*). In three of these cases, the shapes of the measured and theoretical distributions agree very well. However, in the case of the largest sample, obtained from *Lytechinus* spermatozoa at the higher MgATP concentration (Fig. 11 *B*), the agreement is poor. This poor agreement can be described as an excess of low values of doublet separation. Compared to the theoretical curve shown for a diameter of 194 nm, which predicts that 64% of the values of doublet separation should be less than 100 nm, ~75% of the measured values are <100 nm, with a corresponding deficit of values in the range of 100 to 175 nm. If a theoretical curve for a smaller diameter is chosen, an excess of large values, larger than the axonemal diameter, appears. No explanation for this discrepancy, and its appearance in this particular sample, is apparent.

A second test is provided by the values for axonemal diameter obtained by fitting a theoretical distribution to the measured values of doublet separation. There is obviously a large uncertainty in the value of diameter obtained from the measurements on *Lytechinus* spermatozoa at the higher ATP concentration (Fig. 11 *B*), in the range of 160–200 nm. The value of 196 nm for *Lytechinus* spermatozoa at the lower ATP concentration (Fig. 11 *C*) agrees with the upper end of this range. The value for the *Ciona* sperm sample is somewhat higher. However, without measurements on more samples under a wide variety of conditions, it is not reasonable

to attempt to interpret the significance of these differences. Much more serious is the difference between these new values and the smaller value of 132 nm obtained for *Lytechinus* spermatozoa at low MgATP concentration in the previous study (Brokaw, 1989*a*). Although the conditions for sperm reactivation in that study and for the *Lytechinus* sample in Fig. 11 *C* were similar, some difference might have resulted from selection of spermatozoa for analysis. In the earlier study, analysis was restricted to spermatozoa with relatively long straight regions between bends, because measurements of bead separations were only made in straight regions of the flagellum. In the present study, spermatozoa with small head angle oscillations were selected. These samples might therefore be different, but it is difficult to explain why such a difference would give a large difference in diameter. Additionally, the methods used for analysis of bead separations were different in the earlier study. Although it has not been feasible to reexamine the older photographs with the new image analysis methods, examples of both the old and new photographs have been measured by projecting the negatives onto a screen and directly measuring the distances between beads; in both cases the measurements agree adequately with the values obtained from the different image analysis methods used for the two samples. The new analysis methods described in the present paper provide more accurate, and sometimes larger, values of doublet separation for cases where there are differences in phase between two beads of a pair. However, the restriction of the earlier analysis to measurements of bead separations in straight regions between bends should minimize the effect of this difference. Therefore, no explanation is available for the large discrepancy in axonemal diameter indicated by the old and new measurements.

A third test is provided by the uniformity of calculated doublet separations along the length of the flagellum when apparently correct values of shear angle are used, as in Figs. 9 *E* and 10 *F*. The values of doublet separation for the bins in these figures are more uniform than the values in Figs. 9 *F* and 10 *E*, and the relatively low level of noise in these values argues in favor of their accuracy. However, in both cases there is a consistent decrease in calculated diameter along the length of the flagellum, and there is no obvious explanation for this result.

Therefore, all three of these tests identify some problems with the interpretation of the bead separation measurements, which cannot be resolved until measurements on many additional samples are available. However, none of these discrepancies appears to be great enough to cancel out the significant difference observed between the sliding patterns in *Lytechinus* and *Ciona* spermatozoa.

Sliding Patterns in Lytechinus Sperm Flagella

The direct measurements on *Lytechinus* spermatozoa indicate that when the orientation of the sperm head oscillates during the beat cycle there is no corresponding oscillation in the orientation of the basal end of the flagellum. The oscillation of the sperm head is presumably caused by lateral forces resulting from viscous reaction to the side-to-side movement of the head. Gibbons (1982) examined the head trajectories of swimming sea urchin spermatozoa and observed that the angular oscillation was in phase with the side-to-side movement. Photographs of *Lytechinus* spermatozoa under the conditions of the experiments reported here have confirmed this conclusion (not shown). This conclusion can also be described by saying that as the rear end of the sperm head is driven from side to side by the bending of the flagellum, the viscous resistance to movement of the head causes the head to tilt, so that there is very little side-to-side movement of the front end of the head. Tilting of the head with respect to the basal end of the flagellum is consistent with photographs which tend to show that the flagellum emerges from the head at different angles at different times in the beat cycle (see Goldstein, 1976, 1977, 1981). However, such observations cannot distinguish between flexure between the head and the base of the flagellum and bending of the flagellum very close to the basal end. Electron micrographs showing the junction between the sea urchin sperm flagellum and the sperm head (see Sale, 1986) indicate that the basal end of the flagellum is within an indentation in the sperm head, but is attached to the sperm head by a slender filament, which could easily be imagined to be flexible.

If the sea urchin sperm head has a flexible attachment to the basal end of the flagellum and the orientation of the basal end of the flagellum does not oscillate as the spermatozoon swims, then measurement of shear angles relative to an external coordinate system, as, for example, in Fig. 5 of Hiramoto and Baba (1978), can give a more accurate description of microtubule sliding within the sea urchin sperm flagellum. If the bending waves are asymmetric so that the orientation of the spermatozoon rotates with each beat cycle, this rotation must be removed from the measurements of angle relative to an external coordinate system to obtain an accurate description of microtubule sliding. One method used here has been to resolve the measured head angle time series into a sinusoidal oscillation and a linear component, and to use the sinusoidal component to adjust the angles measured relative to the sperm head axis. Alternatively, the linear component of head angle change with time could be used to adjust angles measured relative to an external coordinate system.

When there is no significant angular oscillation of the basal end of the flagellum, the amplitude of sliding is uniform along the length of the flagellum and does not show the mid-region minimum seen in plots such as Fig. 6 *A*. A uniform, or purely metachronous, sliding pattern (Fig. 2 *A*) indicates that the rates of growth of principal and reverse bends in the basal region of the flagellum are equal, so that there is no synchronous sliding in regions of the flagellum distal to the developing bends. The sliding behavior in sperm flagella under these conditions is therefore similar to that seen at low beat frequencies, where there is little or no oscillation of the sperm head, and similar to that seen in cases where the sperm head is fixed, where the shear angle curves reveal little or no oscillatory synchronous sliding (Hiramoto and Baba, 1978; Gibbons, 1982).

These conclusions, based on direct measurements of sliding, therefore reinforce Goldstein's (1976) original suggestion that normal flagellar bend generation in sea urchin sperm flagella occurs by coordinated growth of two bends near the basal end of the flagellum, as shown in Fig. 2 *A*. There is therefore no need to superimpose an oscillatory synchronous sliding on the metachronous sliding associated with bend propagation in distal regions of the flagellum. This means that in symmetric binding waves, bends distal to the

developing bend at the base of the flagellum are separated by interbend regions that are propagating regions of 0 sliding. These interbend regions could conceivably be regions in which sliding is prevented by stable cross-bridges between outer doublet microtubules. This idea is attractive because it provides a simple mechanism for maintaining the bends, in opposition to the elastic bending resistance of the flagellum that will tend to straighten the flagellum. However, the idea of stable cross-bridges in interbend regions is probably inconsistent with the propagation of asymmetric bending waves. In asymmetric bending waves, there is a gradual change in the shear angle of each interbend region as it propagates along the flagellum. Gibbons (1981) has described this as nonoscillatory synchronous sliding. This slow sliding in the interbend regions could either be required to allow the interbend region to propagate along a curved flagellum, or could be responsible for the asymmetry of the bending waves (see Brokaw, 1979; Eshel and Brokaw, 1987).

It is perhaps more important to recognize that Goldstein's (1976) description of bend initiation requires that the sliding behavior in the first interbend region, between the two developing bends, is very different from the sliding behavior in the other interbend regions on the flagellum. Every time that a new bend begins on the flagellum, the behavior of the interbend region between the two previous growing bends changes abruptly to the behavior characteristic of interbend regions between propagating bends. This difference is also strongly demonstrated by experiments in which mechanical vibrations in the normal bending plane are imposed on a spermatozoon held by a micromanipulator, forcing it to vibrate at a higher frequency than its natural beat frequency (Shingyoji et al., 1991). In these experiments, the imposed vibration caused large changes in sliding in the first interbend region, and relatively little change in the behavior of the interbend regions between bends propagating in the distal region of the flagellum. The first interbend might be a region where sliding is activated in only one direction, with sliding activated in both directions in the more distal interbends (Brokaw, 1989*b*). The detailed computer modeling needed to determine whether this difference can explain the pattern of bend development described by Goldstein (1976) has not yet been accomplished.

Sliding Patterns in Ciona Sperm Flagella

In *Ciona* sperm flagella, measurements of shear angle relative to the head and direct measurements of sliding between attached beads agree, indicating that there is no flexure of the sperm head relative to the base of the flagellum. This is consistent with observation that in these spermatozoa, the flagellum often appears to emerge from the head at a fixed angle (see Fig. 3), and that fitting of the region of the flagellum near the base is more successful if the first segment of the flagellar model is given a fixed angle relative to the axis of the sperm head (not shown here). These observations are also consistent with electron microscopical observations indicating that in *Ciona* the base of the sperm flagellum abuts tightly to the sperm nucleus and is offset from the longitudinal axis of the sperm head (Woollacott, 1977).

These observations lead to the conclusions that sliding patterns such as the one in Fig. 6 *A* are correct, and that oscillatory synchronous sliding is a real feature of the sliding pattern of *Ciona* sperm flagella. This oscillatory synchronous sliding could be caused by viscous forces acting on the sperm head and causing it to tilt as its basal end is moved from side to side by the bending of the flagellum. In this case the change in angle of the sperm head would be accommodated by synchronous sliding rather than by flexure between the sperm head and the base of the flagellum. An identical pattern of synchronous sliding could result from internal mechanisms that cause new bends developing at the base of the flagellum to grow in angle less during their second half-cycle than during their first half-cycle, as illustrated in Fig. 2 *C*. Parsimony might dictate the first of these interpretations, to avoid the conclusion that the internal mechanisms for controlling sliding produce synchronous sliding in *Ciona* sperm flagella but not in sea urchin sperm flagella. However, the second interpretation is easier to relate to the damped bending patterns of *Ciona* spermatozoa (Brokaw, 1987, 1989*b*), which indicate a complete failure of the second half-cycle of bend growth. In either case, bend propagation in the distal portion of a flagellum must involve a mechanism that can propagate bends of relatively constant bend angle (Eshel and Brokaw, 1988), in spite of the presence of synchronous sliding. Although bending and bend propagation by a flagellum are the result of active sliding, the regulatory mechanisms may monitor and control bend angle, rather than the local amplitude of sliding. Further investigation of these mechanisms is now facilitated by knowledge that accurate information about the microtubule sliding patterns in *Ciona* spermatozoa can be obtained from measurements of angles relative to the sperm head axis.

I am happy to acknowledge the assistance provided by Sandra Nagayama, Holly Dodson, and Jim Pacheco.

Financial support was provided by National Institutes of Health grants GM-18711, RR-07003 (Biomedical Research Support Grant), AG 08787 (Small Instrumentation Grant [SIG]), and HL 41728 (SIG).

Received for publication 11 March 1991 and in revised form 7 June 1991.

References

Brokaw, C. J. 1971. Bend propagation by a sliding filament model for flagella. *J. Exp. Biol.* 55:289–304.

Brokaw, C. J. 1979. Calcium-induced asymmetrical beating of triton-demembranated sea urchin sperm flagella. *J. Cell Biol.* 82:401–411.

Brokaw, C. J. 1986. Sperm motility. *Methods Cell Biol.* 27:41–56.

Brokaw, C. J. 1987. A lithium-sensitive regulator of sperm flagellar oscillation is activated by cAMP-dependent phosphorylation. *J. Cell Biol.* 105:1789–1798.

Brokaw, C. J. 1989*a*. Direct measurements of sliding between outer doublet microtubules in swimming sperm flagella. *Science (Wash. DC).* 243:1593–1596.

Brokaw, C. J. 1989*b*. Operation and regulation of the flagellar oscillator. *In* Cell Movement: The Dynein ATPases. F. D. Warner, I. R. Gibbons, and P. Satir, editors. Alan R. Liss, Inc., New York. 267–279.

Brokaw, C. J. 1990. Computerized analysis of flagellar motility by digitization and fitting of film images with straight segments of equal length. *Cell Motil. Cytoskeleton.* 17:309–316.

Brokaw, C. J., and B. Benedict. 1968. Mechanochemical coupling in flagella II. Effects of viscosity and thiourea on metabolism and motility of *Ciona* spermatozoa. *J. Gen. Physiol.* 52:283–299.

Brokaw, C. J., and I. R. Gibbons. 1975. Mechanisms of movements in flagella and cilia. *In* Swimming and Flying in Nature. T. Y. Wu, C. J. Brokaw, and C. Brennan, editors. Plenum Publishing Corp., New York. 89–126.

Brokaw, C. J., S. F. Goldstein, and R. L. Miller. 1970. Recent studies on the motility of spermatozoa from some marine invertebrates. *In* Comparative Spermatology. B. Baccetti, editor. Academic Press, New York. 475–485.

Brokaw, C. J., and S. M. Nagayama. 1985. Modulation of the asymmetry of sea urchin sperm flagellar bending by calmodulin. *J. Cell Biol.* 100:1875–1883.

Eshel, D., and C. J. Brokaw. 1987. New evidence for a "biased baseline" mechanism for calcium-regulated asymmetry of flagellar bending. *Cell Motil. Cytoskeleton.* 7:160–168.

Eshel, D., and C. J. Brokaw. 1988. Determination of the average shape of fla-

gellar bends: A gradient curvature model. *Cell Motil. Cytoskeleton.* 9:312–324.
Gibbons, I. R. 1981. Transient flagellar waveforms during intermittent swimming in sea urchin sperm. II. Analysis of tubule sliding. *J. Muscle Res. Cell Motil.* 2:83–130.
Gibbons, I. R. 1982. Sliding and bending in sea urchin sperm flagella. *Symp. Soc. Exp. Biol.* 35:225–287.
Gibbons, I. R. 1986. Transient flagellar waveforms in reactivated sea urchin sperm. *J. Muscle Res. Cell Motil.* 7:245–250.
Goldstein, S. F. 1976. Form of developing bends in reactivated sperm flagella. *J. Exp. Biol.* 64:173–184.
Goldstein, S. F. 1977. Asymmetric waveforms in echinoderm sperm flagella. *J. Exp. Biol.* 71:157–170.
Goldstein, S. F. 1981. Motility of basal fragments of sea urchin sperm flagella. *J. Cell Sci.* 50:65–77.
Hiramoto, Y., and S. A. Baba. 1978. A quantitative analysis of flagellar movement in echinoderm spermatozoa. *J. Exp. Biol.* 76:85–104.
Omoto, C. K., and C. J. Brokaw. 1982. Structure and behaviour of the sperm terminal filament. *J. Cell Sci.* 58:385–409.
Sale, W. F. 1986. The axonemal axis and Ca^{2+}-induced asymmetry of active microtubule sliding in sea urchin sperm tails. *J. Cell Biol.* 102:2042–2052.
Satir, P. 1968. Studies on cilia. III. Further studies on the cilium tip and a "sliding filament" model of ciliary motility. *J. Cell Biol.* 39:77–94.
Shingyoji, C., I. R. Gibbons, A. Murakami, and K. Takahishi. 1991. Effect of imposed head vibration on the stability and waveform of flagellar beating in sea urchin spermatozoa. *J. Exp. Biol.* 156:63–80.
Silvester, N. R., and M. E. J. Holwill. 1972. An analysis of hypothetical flagellar waveforms. *J. Theor. Biol.* 35:505–523.
Warner, F., and P. Satir. 1974. The structural basis of ciliary bend formation. Radial spoke positional changes accompanying microtubule sliding. *J. Cell Biol.* 63:35–63.
Woollacott, R. M. 1977. Spermatozoa of *Ciona intestinalis* and analysis of ascidian fertilization. *J. Morphol.* 152:77–88.